TECHNICAL NOTE

D-967

MEASUREMENT AND EMPIRICAL CORRELATION

OF TRANSPIRATION-COOLING PARAMETERS ON A 25° CONE

IN A TURBULENT BOUNDARY LAYER IN BOTH FREE FLIGHT

AND A HOT-GAS JET

By Thomas E. Walton, Jr., and Bernard Rashis

Langley Research Center
Langley Air Force Base, Va.

NATIONAL AERONAUTICS AND SPACE ADMINISTRATION

WASHINGTON   October 1961

NATIONAL AERONAUTICS AND SPACE ADMINISTRATION

TECHNICAL NOTE D-967

MEASUREMENT AND EMPIRICAL CORRELATION

OF TRANSPIRATION-COOLING PARAMETERS ON A 25° CONE

IN A TURBULENT BOUNDARY LAYER IN BOTH FREE FLIGHT

AND A HOT-GAS JET

By Thomas E. Walton, Jr., and Bernard Rashis

SUMMARY

Transpiration-cooling parameters are presented for a turbulent boundary layer on a cone configuration with a total angle of 25° which was tested in both free flight and in an ethylene-heated high-temperature jet at a Mach number of 2.0. The flight-tested cone was flown to a maximum Mach number of 4.08 and the jet tests were conducted at stagnation temperatures ranging from 937° R to 1,850° R. In general, the experimental heat transfer was in good agreement with the theoretical values. Inclusion of the ratio of local stream temperature to wall temperature in the nondimensional flow rate parameter enabled good correlation of both sets of transpiration data. The measured pressure at the forward station coincided with the theoretical pressure over a sharp cone; however, the measured pressure increased with distance from the nose tip.

INTRODUCTION

Previous experimental investigations (refs. 1 and 2) have indicated that transpiration-cooling techniques have considerable merit as a cooling or heat-blocking system. To date, investigations of this system have been conducted only in ground facilities.

This paper presents the transpiration-cooling results obtained in free flight with a cone configuration having a 25° total angle which was flown to a maximum Mach number of 4.08 using nitrogen as the coolant. Also presented are results obtained from a model approximately one-half the size of the flight model which was tested in an ethylene-heated high-temperature jet at a Mach number of 2.0 and at stagnation temperatures ranging from 937° R to 1,850° R using helium as the coolant. The results

from both tests were correlated by the inclusion of the ratio of local stream temperature to wall temperature in the nondimensional flow rate parameter.

SYMBOLS

c	specific heat of skin material, $Btu/lb/^{\circ}F$	
C_p	pressure coefficient	L
		1
$c_{p,c}$	specific heat at a constant pressure of the coolant, $Btu/lb/^{\circ}F$	7
		1
$c_{p,l}$	specific heat at a constant pressure of the air, $Btu/lb/^{\circ}F$	1
F	ratio of coolant weight flow rate to local weight flow rate, $G_c/(\rho V)_l$	
G	weight flow rate, $lb/(sq\ ft)(sec)$	
h	heat-transfer coefficient, $Btu/(sq\ ft)(sec)(^{\circ}F)$	
k	thermal conductivity, $Btu/(sq\ ft)(sec)(^{\circ}F/ft)$	
M	Mach number	
N_{Pr}	Prandtl number	
N_{St}	Stanton number	
Δp	pressure drop across porous conical half	
q	heating rate, $Btu/(sq\ ft)(sec)$	
R	Reynolds number, per ft	
T	temperature	
t	time, sec	
V	velocity, ft/sec	
w	specific weight of skin material, $lb/cu\ ft$	
ρ	specific weight of air, $lb/cu\ ft$	
τ	skin thickness, ft	

Subscripts:

c	coolant values
l	local values
pw	porous-wall values
r	recovery values
s	outside surface values
t	stagnation values
∞	free-stream values
0	theory for $G_c = 0$

L
1
7
1
1

FLIGHT MODEL

Model Configuration

The flight-model configuration was a 25° cone having a 0.19-inch nose tip radius and a 10.25-inch base diameter followed by a 34.70-inch-long cylindrical section. Figure 1 is a sketch of the model showing the pertinent construction details and dimensions. A photograph of the model and third stage is shown in figure 2.

The model cone consisted of two halves, a porous half through which the coolant passed and a nonporous or solid half. The solid half was rolled from type 347 stainless steel 0.093 inch in thickness. The porous half was rolled from 1/8-inch-thick sintered powdered stainless-steel sheet. The two conical halves and the solid stainless-steel nose tip were fastened together by means of welded butt joints. The solid half was sealed off from the porous half by means of a steel baffle.

Preliminary check tests indicated that a coolant-flow-rate gradient existed along the porous half of the cone which was caused by the enlargement of the pores when the porous half was rolled to its conical shape. In order to alleviate this condition, the porous stainless-steel half was coated with molybdenum by a flame-spraying process. Further check tests were made by dividing the porous area of the cone into eight equal segments and measuring the coolant flow rate at the same test conditions through each segment. The coolant flow rate through any one segment was found to be within ± 3 percent of the average value for all the segments.

Cooling System

A schematic diagram of the model and cooling system is shown in figure 3. The nitrogen coolant was stored in two modified hydraulic accumulators at a gage pressure of 1,500 psi. The nitrogen coolant was kept in check by means of an explosive type of valve. Briefly, the normally closed explosive valve holds pressure with no leakage by its solid diaphragm which is machined as an integral part of the valve body. The diaphragm is sheared out when the explosive squib is fired allowing nitrogen coolant to pass unobstructed through the valve. A high-pressure flow regulator was used to throttle the nitrogen coolant from the high accumulator pressure to a lower working pressure.

The technique employed for determining nitrogen coolant flow rates involved the measurement of model cone surface pressure and differential pressure Δp across the porous half of the model cone. A calibration was made in a vacuum chamber which correlated these two variables with the measured coolant flow rate. The measurement of the coolant flow rate during the calibration procedure was accomplished by replacing the explosive valve (fig. 3) with a solenoid-operated gate valve, a flow meter, a pressure transducer, and a thermocouple. The resulting calibration curves are shown in figure 4.

Instrumentation

A 10-channel telemeter, which was located just behind the cooling system (fig. 3) transmitted four channels of pressures, two channels of temperatures, and one channel each of normal, transverse, thrust, and drag accelerations. Twenty-four thermocouples (12 per channel) were installed in the model at the locations shown in figure 1. Eleven of these were made of No. 30 gage chromel-alumel and were spot welded to the back side of the solid conical half. Eleven thermocouples were spot welded to the porous half and were made of iron-constantan. Two iron-constantan thermocouples (23 and 24) were fastened to the 3/4-inch steel tubing inside the model and were used for measuring the nitrogen coolant temperature.

During flight, the commutation arrangement was such that each temperature measurement was recorded approximately 5 times per second. Three standard voltages were also commutated at the same rate on each of the two thermocouple channels for an inflight calibration. These were equivalent to the lowest, middle, and highest temperatures that the skin was anticipated to reach.

Three pressure orifices were installed on the surface of the solid conical half and were equally spaced along a meridian which was 20° from the meridian on which the thermocouples were located as shown in

section A-A of figure 1. Two pressure orifices (4 and 5) were located
inside the model cone. Pressure orifices 2 and 4 were used for measuring
the differential pressure across the porous half of the cone and orifice 5
was used for measuring the model chamber pressure. Orifices 1 and 3 were
used for measuring surface pressure. It was assumed that the surface
pressure measured on the solid side was the same as the surface pressure
on the porous side at 0° angle of attack.

Other instrumentation consisted of ground-based radar units for
measuring model velocity and for obtaining the location of the model
in space.

L
1
7
1
1

Atmospheric data and wind conditions were measured to an altitude
of 95,000 feet by means of a radiosonde launched near the time of flight
and tracked by Rawin set AN/GMD-1A.

Propulsion System

The propulsion system consisted of three stages of solid-propellant
rocket motors. The first and second stages were an M6 JATO rocket motor
(Honest John) and M5 JATO rocket motor (Nike), respectively. The third
stage was a British Series D 2.5 ES 24,000 B rocket motor (Gosling).
A photograph of the model and propulsion system is shown in figure 5.

Flight-Test Procedure

The model was ground launched at an elevation angle of 77° along
an azimuth angle of 130°. A plot of the flight trajectory and sequence
of events is shown in figure 6. The first stage or Honest John rocket
motor burned for about 5 seconds and drag separated immediately from the
remaining two stages. A coast period of approximately 33 seconds followed
allowing the remaining two stages to reach the desired altitude. A
mechanical timer was used to actuate the cooling system and ignite the
last two stages. At 37.6 seconds the second stage or Nike fired and at
the same time the nitrogen cooling system was actuated. At Nike burnout
(41.3 seconds) a delay squib ignited the last stage or Gosling motor.
During the burning of the Gosling motor the vehicle became unstable and
pitch oscillations were observed 0.2 second after Gosling ignition. No
data are presented after 41.5 seconds and failure of the telemeter signal
occurred at 43.2 seconds.

The variation of free-stream static temperature and pressure as
determined from the radiosonde measurements for the flight trajectory
is shown in figure 7 along with the calculated variation of the flight
stagnation temperature. Time histories of flight velocity and altitude

are shown in figure 8 and free-stream Mach number and free-stream Reynolds number per foot for the flight trajectory are shown in figure 9.

GROUND-TESTS MODEL

The ground-tests model configuration was a 25° cone having a $3/32$-inch nose tip radius and a $4\frac{1}{2}$-inch base diameter followed by a $4\frac{1}{8}$-inch-long cylindrical afterbody section. Figure 10 is a sketch of the model showing the pertinent construction details and dimensions. Figure 11 is a photograph of the model and test sting.

The ground-tests model cone also consisted of two halves. The nonporous or solid half was rolled from $3/32$-inch-thick Inconel sheet. The porous half was rolled from $3/32$-inch-thick sintered powdered stainless-steel sheet. The two conical halves were fastened together by means of welded butt joints. The solid half was sealed off from the porous half by two steel baffles. The cylindrical afterbody and sting support were both water cooled.

No coolant-flow-rate gradient was observed along the porous conical half of the ground model; consequently, it was not flame sprayed.

Cooling System and Instrumentation

A schematic diagram of the ground-test model and cooling system is shown in figure 12. A pressure gage, a thermocouple, and a flow meter were installed in the coolant supply line for measuring the mass flow of helium coolant.

The model was instrumented with 14 thermocouples and five pressure orifices at the locations shown in figure 10. Seven of the thermocouples were made of No. 30 gage chromel-alumel and were spot welded to the inside surface of the nonporous or solid half. In addition, the solid half was instrumented with four pressure orifices. Seven No. 30 gage chromel-alumel thermocouples were also spot welded to the inside surface of the porous half. A fifth pressure orifice was located inside the model.

Test Facility and Procedure

The ground tests were conducted in the ethylene-heated high-temperature jet of the NASA Wallops Station. This facility is.capable of producing a hot jet having a free-stream Mach number of 2.0 at a

pressure of 1 atmosphere and stagnation temperatures up to 3,500° F.
A detailed description of the physical characteristics of this facility
is given in reference 3.

The model was mounted on a side-injection type of sting at 0° angle
of attack and yaw (fig. 11) and was inserted into the jet stream only
after steady flow conditions were established. The solenoid valve was
programed to open and allow helium coolant to flow through the model
several seconds before the model entered the jet stream.

RESULTS AND DISCUSSION

Temperature Data

Figure 13 presents the measured temperature distribution along
both the solid and porous conical halves for several times during the
flight test. Typical time histories of the outside and inside surface
temperatures for the solid and porous conical halves are presented in
figures 14(a) and 14(b), respectively. The temperature gradient through
the solid conical half was calculated by the method described in ref-
erence 4. Since the coolant temperature was much lower than the porous
wall temperature, the passage of coolant through the porous wall contrib-
uted to a temperature gradient through the porous conical half. The
equation for computing the temperature difference ΔT between the
outside and inside surfaces of the porous half given in the form
(obtained from ref. 5)

$$\frac{\Delta T}{T_r - T_c} = \frac{\dfrac{N_{St} c_{p,l}}{F c_{p,c}}}{1 + \dfrac{N_{St} c_{p,l}}{F c_{p,c}}} \left[1 - \exp\left(- \frac{G_c c_{p,c} \tau}{k_{pw}} \right) \right]$$

and modified for convenience to the form

$$\frac{\Delta T}{T_r - T_c} = \frac{\dfrac{T_s - T_c}{T_r - T_s}}{1 + \dfrac{T_s - T_c}{T_r - T_s}} \left[1 - \exp\left(- \frac{G_c c_{p,c} \tau}{k_{pw}} \right) \right]$$

was solved by an iteration process where the recovery temperature T_r was computed from the relation (for no coolant flow)

$$T_r = N_{Pr}^{1/3}(T_t - T_l) + T_l$$

Although reference 2 indicates that recovery temperature (with transpiration) is a function of coolant flow rate, the deviation of the recovery temperature from the value for no coolant flow is negligibly small and was not considered in the present results.

The outside surface temperature of the porous half obtained by adding the calculated values of ΔT to the measured inside surface temperature is shown in figure 14(b) as a function of time. Temperature data beyond 41.5 seconds were disregarded because of the pitch oscillations observed during this portion of the flight.

Pressure Data

Figure 15(a) shows the measured chamber pressure, differential pressure across the porous conical half ΔP, and average surface pressure as a function of time on the flight model cone. The coolant flow rates shown in figure 15(b) as a function of time were obtained from the calibration curves (fig. 4) which correlate the mass flow of nitrogen coolant with cone surface pressure and Δp. In addition to cone surface pressure and ΔP the mass flow rate of nitrogen coolant is also a function of temperature. Since the coolant gas was discharged through the porous conical half during flight in the same temperature range as the calibration tests in the vacuum chamber, no temperature correction was applied to the mass flow rate.

Pressure Coefficient

The measured surface pressures on the flight-test cone at the locations shown were reduced to pressure coefficients and the data are presented as a function of Mach number in figure 16. Also shown are the theoretical results for a 25° total angle cone from reference 6.

Examination of the data shows an increase in pressure with distance from the nose tip as the Mach number increases. The measured pressure at station 1 was in good agreement with the theoretical results; however, the pressure measured at station 3 was higher than the theoretical results.

Heat Transfer

Heating rates on the solid conical half of the flight-test cone were computed by

$$q = w\tau c \frac{dT}{dt}$$

where c, the specific heat, was evaluated at the average wall temperature, and dT/dt is the slope of the curve of average wall temperature against time.

The local heat-transfer coefficient was computed from the relation

$$h = \frac{q}{T_r - T_s}$$

where T_r and T_s are the recovery temperature for no coolant flow and the computed outside surface temperature, respectively. The heat-transfer results along the solid conical half are presented as nondimensional Stanton number evaluated at local conditions. Longitudinal heat conduction within the solid conical half was computed and found to be negligibly small.

Figure 17 is a plot of the Stanton number variation along the solid conical half of the flight model for several times during the flight test. Also shown are the theoretical values for laminar and turbulent heat transfer taken from references 7 and 8, respectively, and corrected for conical flow according to reference 9. Examination of the data indicates that transition occurred at a location forward of the 4.0-inch station. The Reynolds number variation at the 4.0-inch station for the data shown in figure 17 was from 2.26×10^6 to 2.65×10^6.

The experimental data between stations at 11.5 inches to 21.5 inches from 40.5 seconds to 41.5 seconds were generally in good agreement with turbulent theory. Experimental data beyond 41.5 seconds were disregarded because of the pitch oscillations observed during this portion of the flight.

Figure 18(a) shows the variation of the cooling efficiency parameter $\frac{T_s - T_c}{T_r - T_c}$ as a function of the nondimensional flow parameter $\frac{F}{N_{St,0}} \frac{c_{p,c}}{c_{p,l}}$ for several times during the flight test. It should be

noted that the flight data were transient and were converted to equilibrium or steady-state values by the method given in reference 10. Also shown are the theoretical values for a turbulent boundary layer $(T_l/T_S = 1)$ given in the form (obtained from ref. 2)

$$\frac{N_{St}}{N_{St,0}} = \frac{\dfrac{F}{N_{St,0}} \dfrac{c_{p,c}}{c_{p,l}}}{\exp\left(\dfrac{F}{N_{St,0}} \dfrac{c_{p,c}}{c_{p,l}}\right) - 1}$$

and modified to the form

$$\frac{T_s - T_c}{T_r - T_c} = \frac{\dfrac{N_{St}}{N_{St,0}}}{\dfrac{N_{St}}{N_{St,0}} + \dfrac{F}{N_{St,0}} \dfrac{c_{p,c}}{c_{p,l}}}$$

The flight data shown in figure 18(a) indicate slightly less reduction in the wall temperature than the results computed from the theory of reference 2.

Figure 18(b) shows the variation of the cooling efficiency parameter, $\dfrac{T_s - T_c}{T_r - T_c}$ as a function of the nondimensional flow parameter $\dfrac{F}{N_{St,0}} \dfrac{c_{p,c}}{c_{p,l}}$ for both the flight data and ground-tests data. The present results show a greater reduction in wall temperature than the results computed from the theory of reference 2 for values of T_l/T_s greater than 1. However, for values of T_l/T_s less than 1 the reverse is seen to be true. It is seen that the effectiveness of transpiration in reducing the heat transfer increases with increases in both the mass flow rate and with T_l/T_s for the present results.

The results from both tests were correlated by the inclusion of the ratio of local stream temperature to wall temperature in the nondimensional flow rate parameter. It was found that by multiplying $\dfrac{F}{N_{St,0}} \dfrac{c_{p,c}}{c_{p,l}}$ by the ratio $(T_l/T_s)^{1.3}$ the values of the cooling efficiency parameter $\dfrac{T_s - T_c}{T_r - T_c}$ fell on a single curve as shown in figure 19. Reference 10 gives the correlation for several other types of boundary

layers by the same method. For example, $(T_l/T_s)^{0.095}$ was found to be the correlating factor for a two-dimensional laminar boundary layer, whereas $(T_l/T_s)^{1.3}$ correlates the present results for a three-dimensional turbulent boundary layer.

CONCLUDING REMARKS

L
1
7
1
1

Transpiration-cooling parameters are presented for a turbulent boundary layer in both free flight and in an ethylene-heated high-temperature jet at a Mach number of 2.0 on a cone configuration having a 25° total angle. The jet tests were conducted at stagnation temperatures ranging from 937° R to 1,850° R. The flight-test model was flown to a maximum Mach number of 4.08.

A reduction of aerodynamic heat transfer was achieved by transpiration cooling; the greater reduction occurred when the wall temperature was less than the local stream temperature.

The flight-test data were correlated with the ground-tests data by the inclusion of the ratio of local stream temperature to wall temperature in the nondimensional flow rate parameter.

Langley Research Center,
        National Aeronautics and Space Administration,
                Langley Air Force Base, Va., August 7, 1961.

REFERENCES

1. Rashis, Bernard: Exploratory Investigation of Transpiration Cooling of a 40° Double Wedge Using Nitrogen and Helium as Coolants at Stagnation Temperature From 1,295° F to 2,910° F. NASA TN D-721, 1961. (Supersedes NACA RM L57F11.)

2. Leadon, B. M., and Scott, C. J.: Measurement of Recovery Factors and Heat Transfer Coefficients With Transpiration Cooling in a Turbulent Boundary Layer at M = 3.0 Using Air and Helium as Coolants. Res. Rep. No. 126 (Contract AF 18 (600)-1226), Inst. Tech., Dept. Aero. Eng., Univ. of Minnesota, Feb. 1956.

3. English, Roland D., Spinak, Abraham, and Helton, Eldred H.: Physical Characteristics and Test Conditions of an Ethylene-Heated High-Temperature Jet. NACA TN 4182, 1958.

4. Coulbert, C. D., MacInnes, W. F., Ishimoto, T., Bussell, B., and Ambrosio, A.: Temperature Response of Infinite Flat-Plates and Slabs to Heat Inputs of Short Duration at One Surface. Contract No. AF33 (038)-14381, Dept. Eng., Univ. of California, Apr. 1951.

5. Hyman, Seymour C.: A Note on Transpiration Cooling. Jet Propulsion, vol. 26, no. 9, Sept. 1956, p. 780.

6. Ames Research Staff: Equations, Tables, and Charts for Compressible Flow. NACA Rep. 1135, 1953. (Supersedes NACA TN 1428.)

7. Van Driest, E. R.: Investigation of Laminar Boundary Layer in Compressible Fluids Using the Crocco Method. NACA TN 2597, 1952.

8. Lee, Dorothy B., and Faget, Maxime A.: Charts Adapted From Van Driest's Turbulent Flat-Plate Theory for Determining Values of Turbulent Aerodynamic Friction and Heat-Transfer Coefficients. NACA TN 3811, 1956.

9. Van Driest, E. R.: The Problem of Aerodynamic Heating. Aero. Eng. Rev., vol. 15, no. 10, Oct. 1956, pp. 26-41.

10. Rashis, Bernard, and Hopko, Russell N.: An Analytical Investigation of Ablation. NASA TM X-300, 1960.

L
1
7
1
1
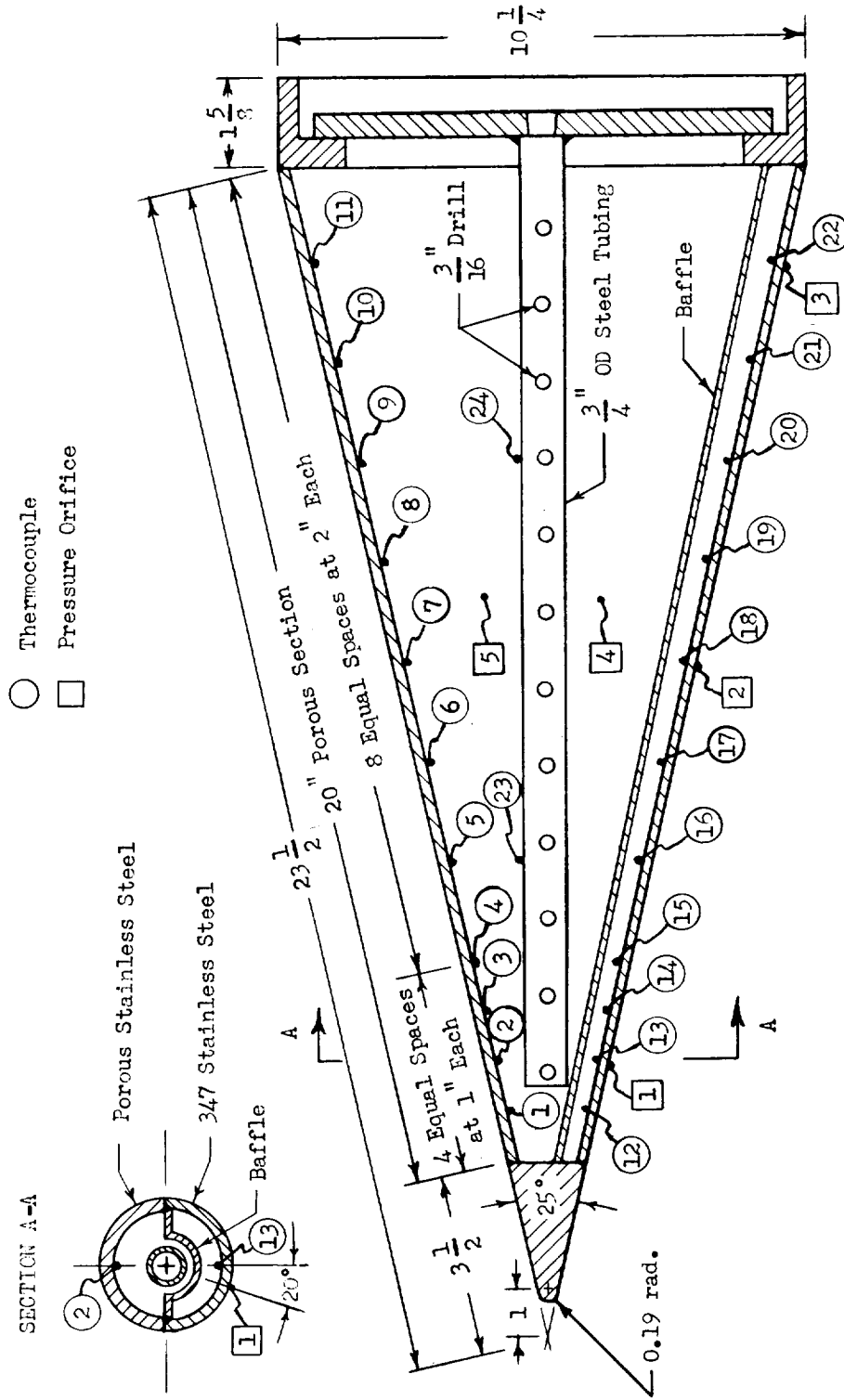
Figure 1.- Sketch of model cone showing construction details and location of instrumentation. All dimensions are in inches.
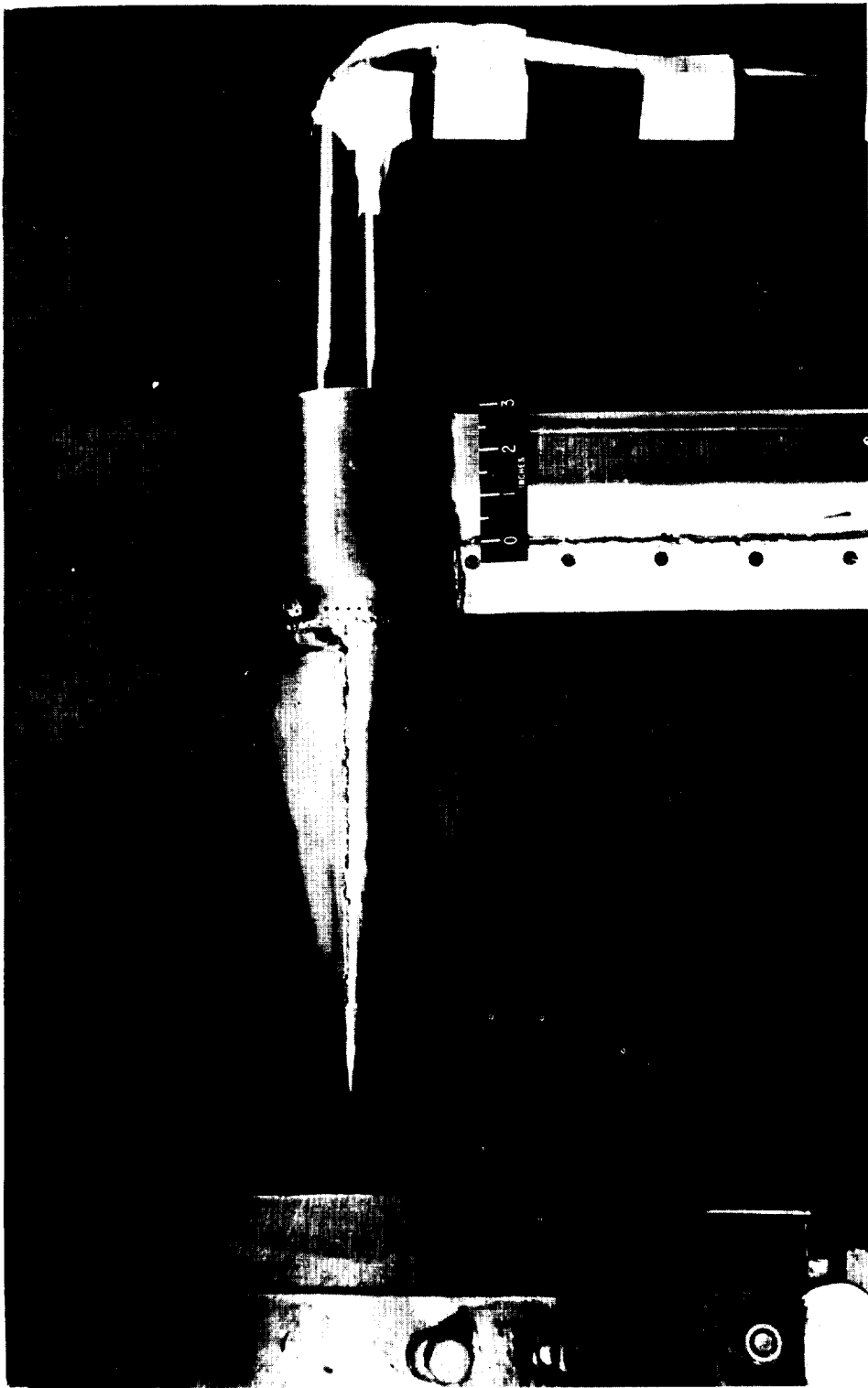
14
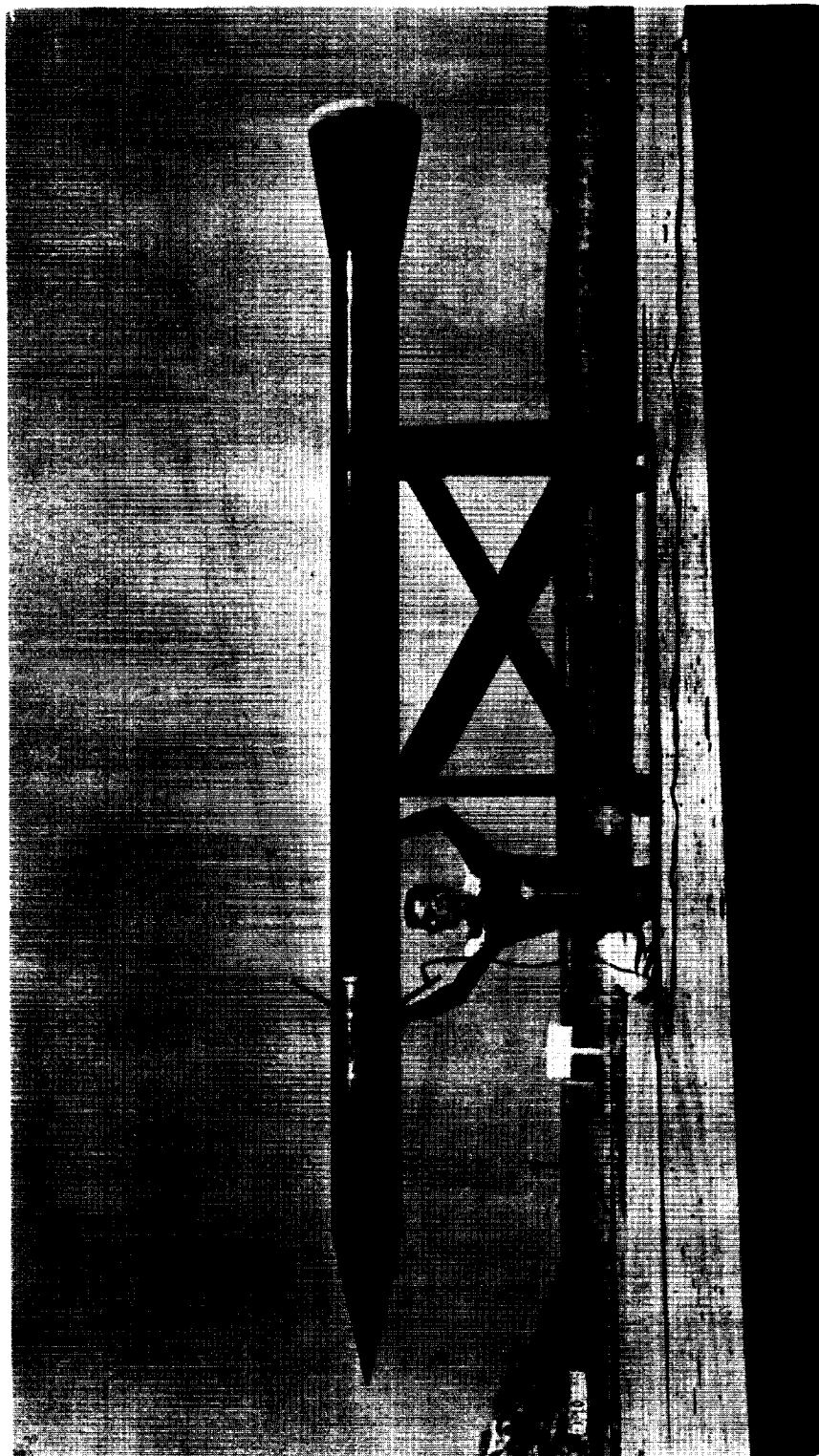
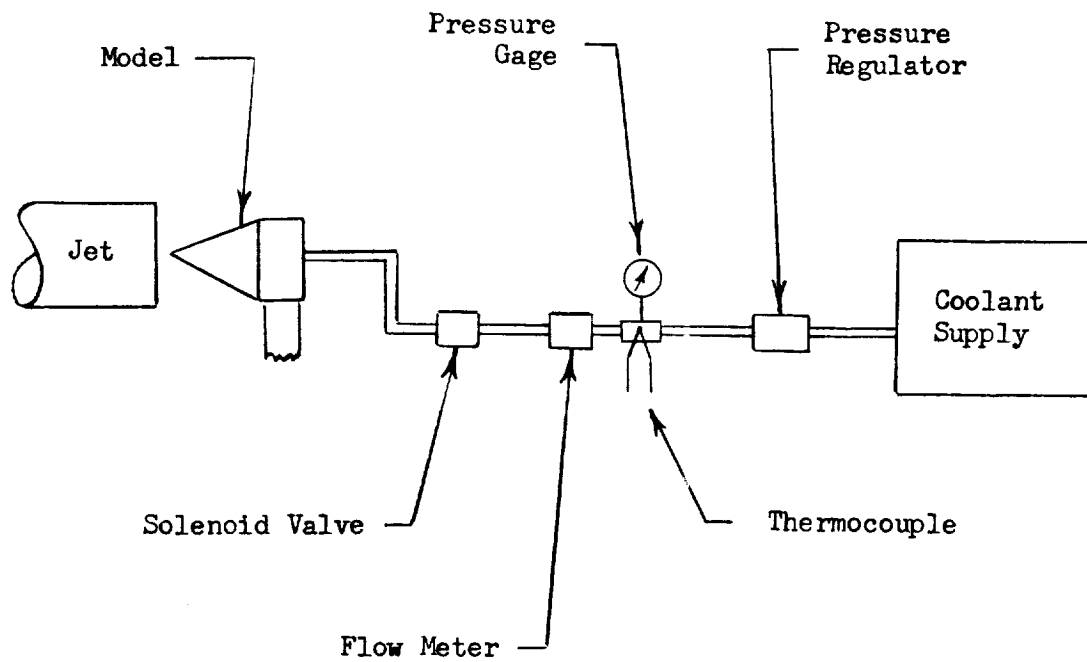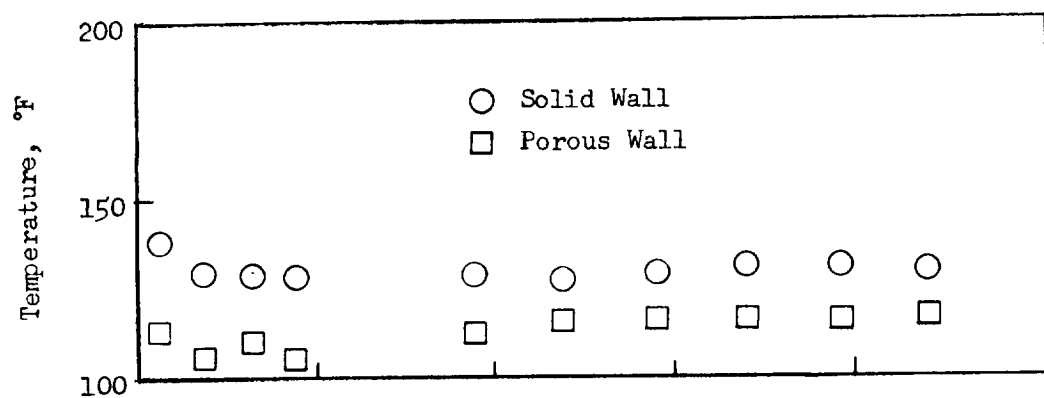
Figure 2.- Photograph of model and third stage.   L-60-2921

L-171L

L-1711

Station 0   Station 24.7"   Station 46.2"   Station 59.4"

Nose
Tip

Porous
Half

Solid
Half

Flow
Regulator

Accumulators

Explosive
Valve

Telemeter Package

Gosling
Motor

Antenna
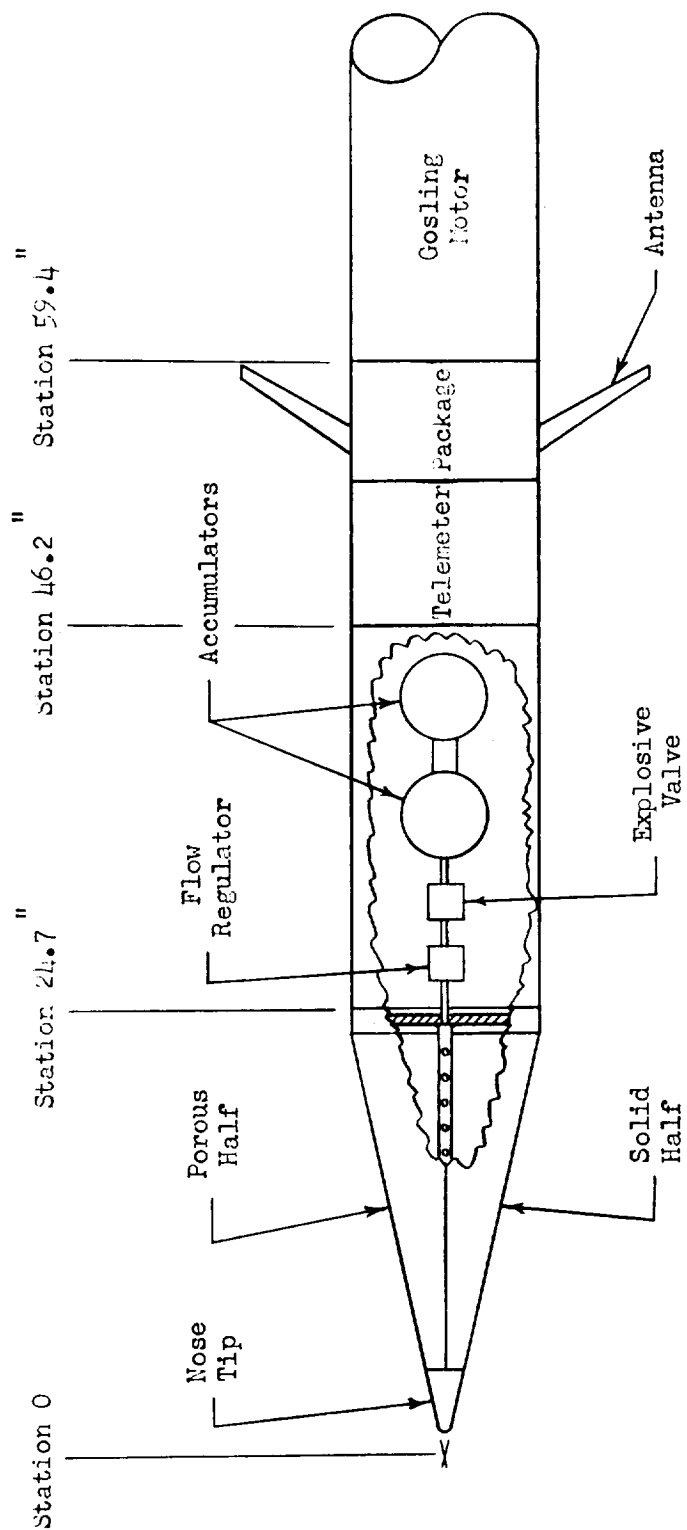
Figure 3.- Schematic diagram of nitrogen cooling system.
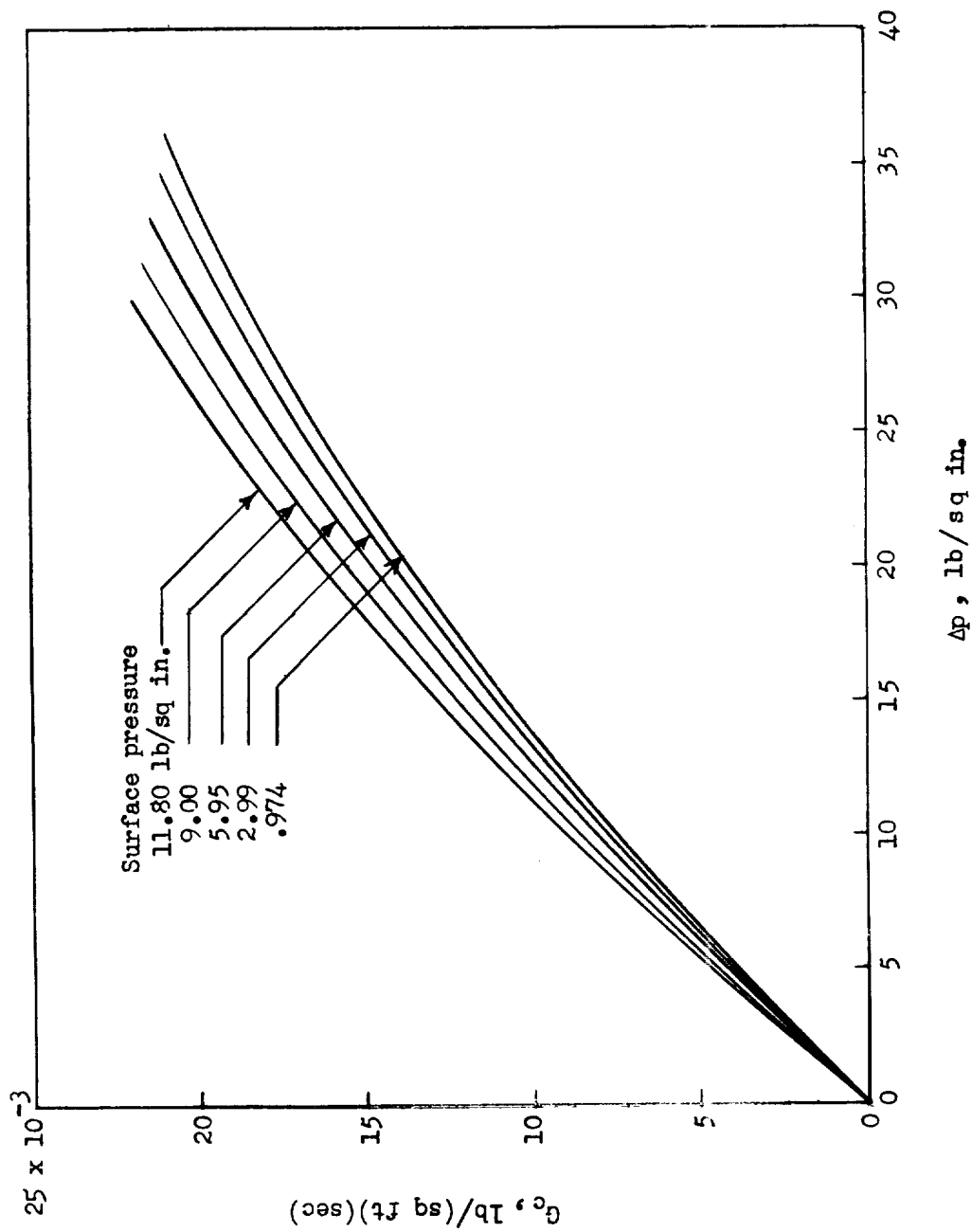
Figure 4.- Mass flow rate of nitrogen coolant as a function of Δp for several cone surface pressures.

L-1711

L-1711
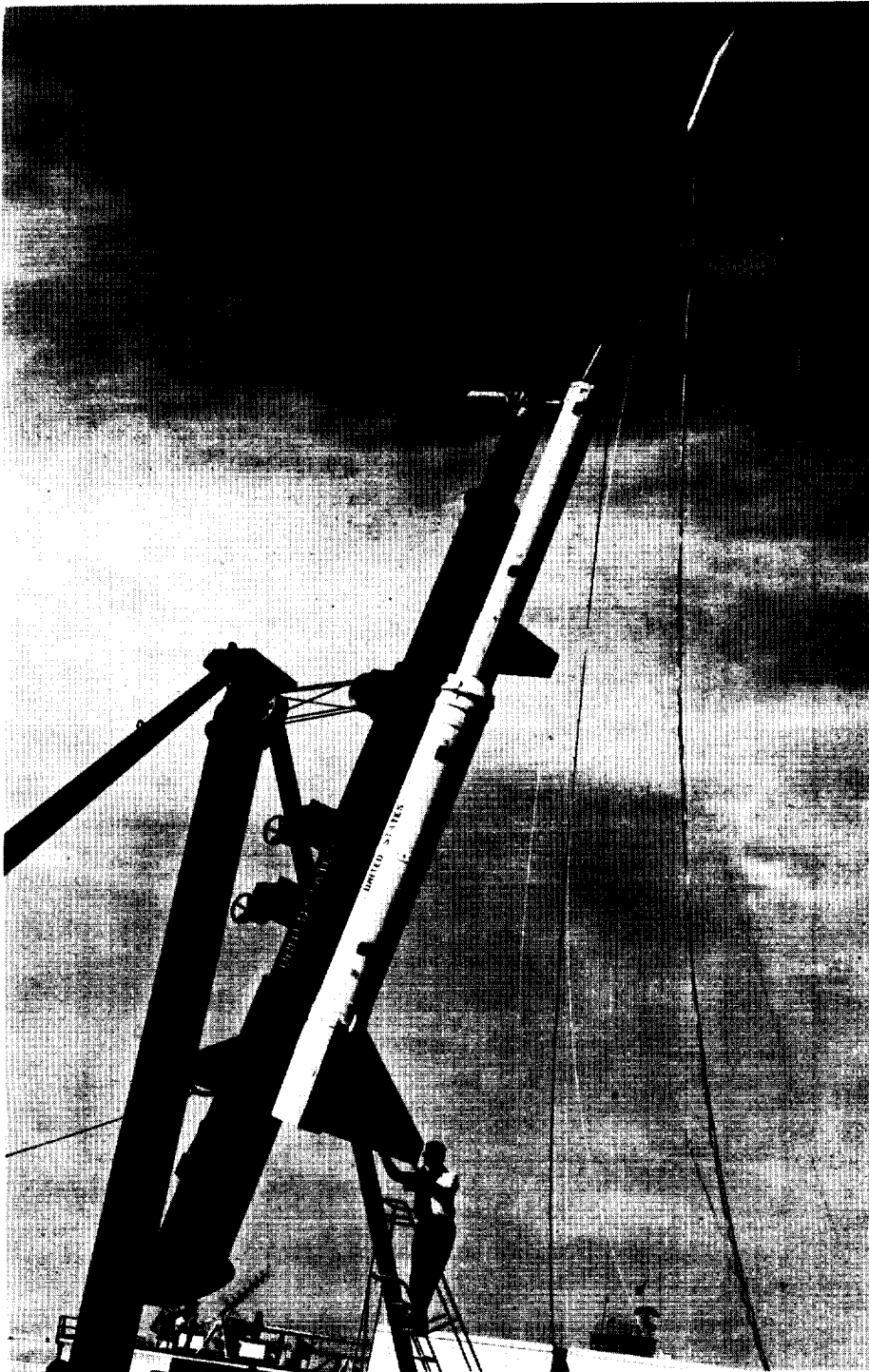
Figure 5.- Photograph of model and boosters on launcher.   L-60-2919
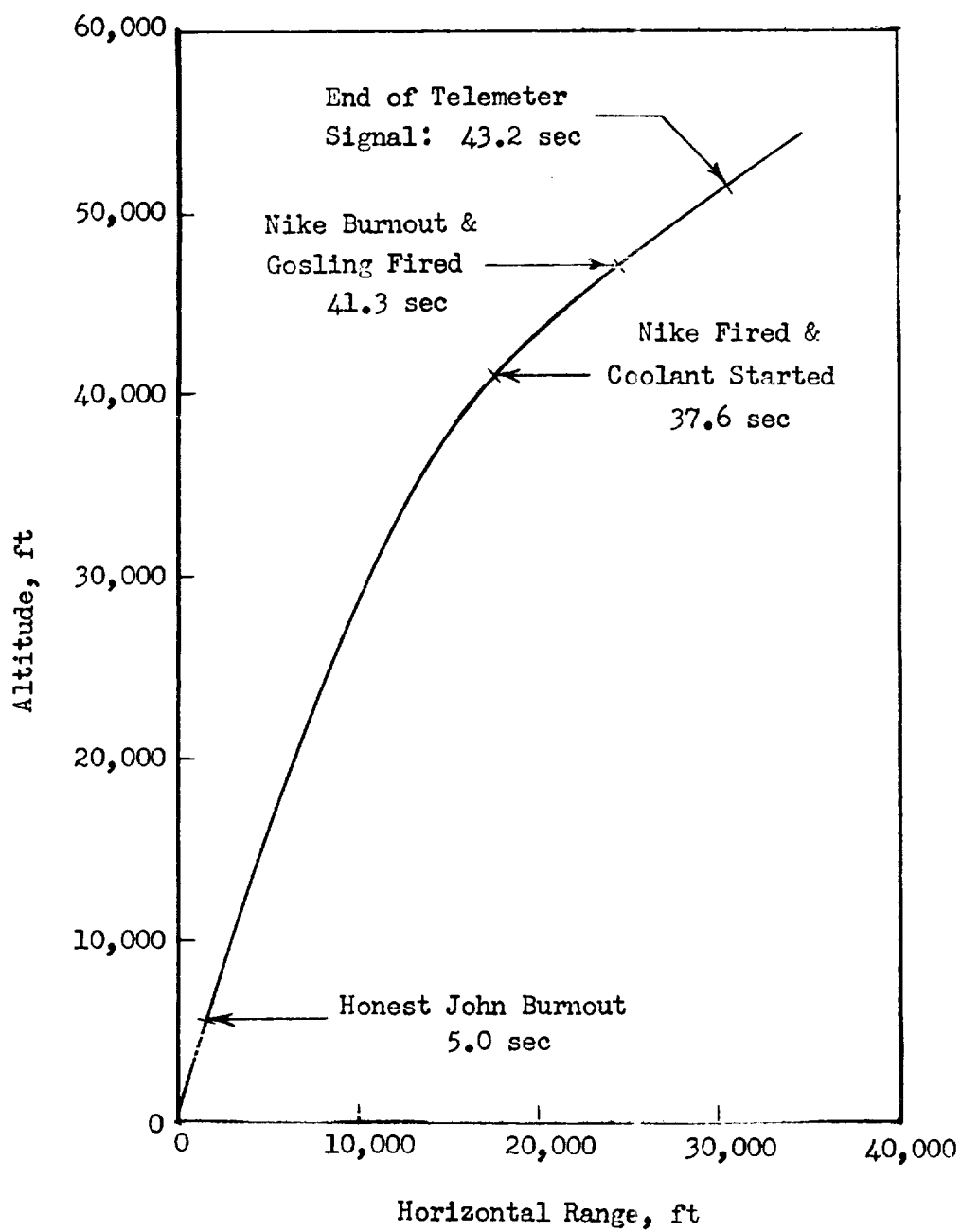
Figure 6.- Flight trajectory.

L-1711
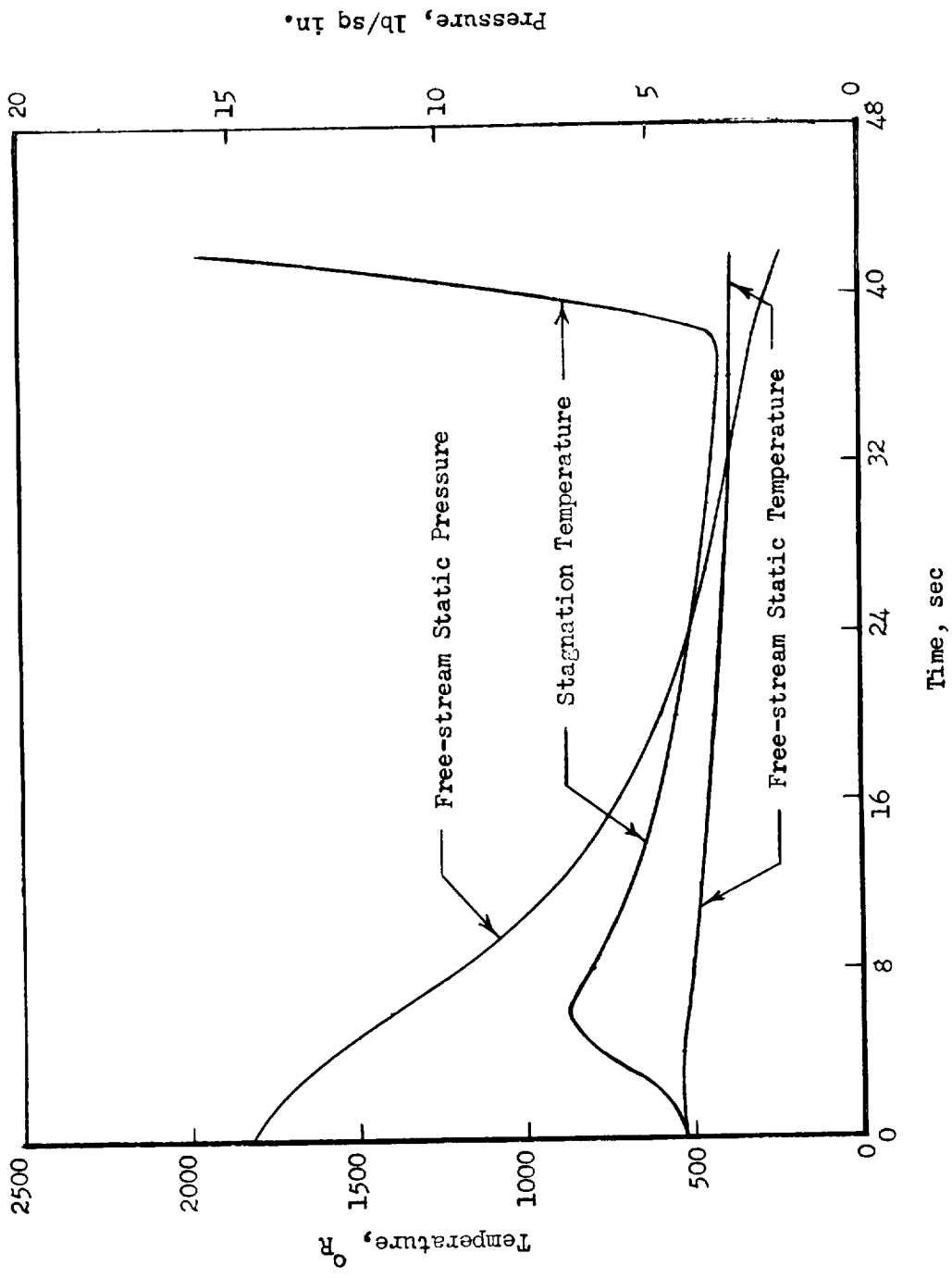
Figure 7.- Free-stream static temperature and pressure and stagnation temperature for model flight trajectory.
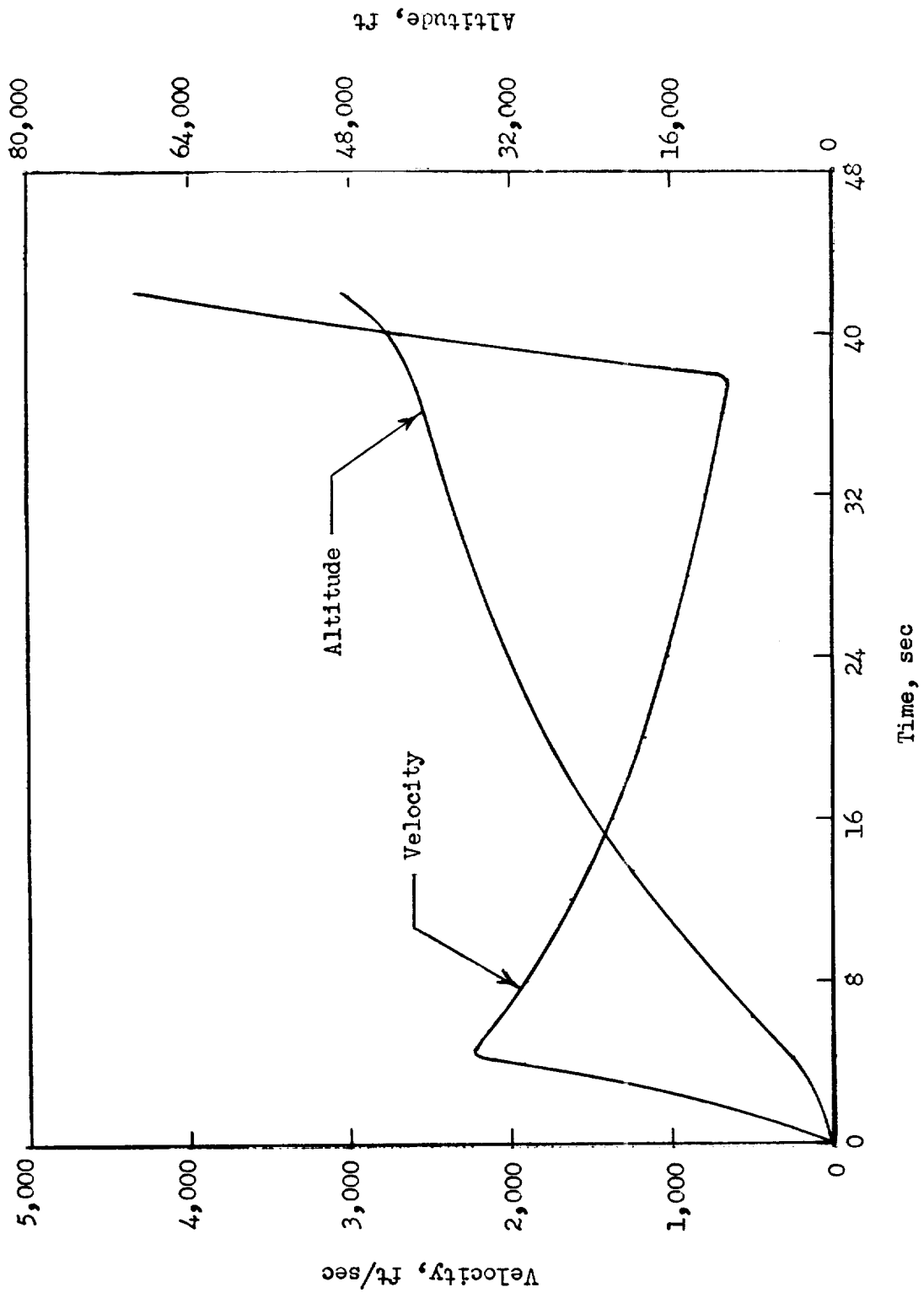
Figure 8.- Altitude and velocity for model flight trajectory.
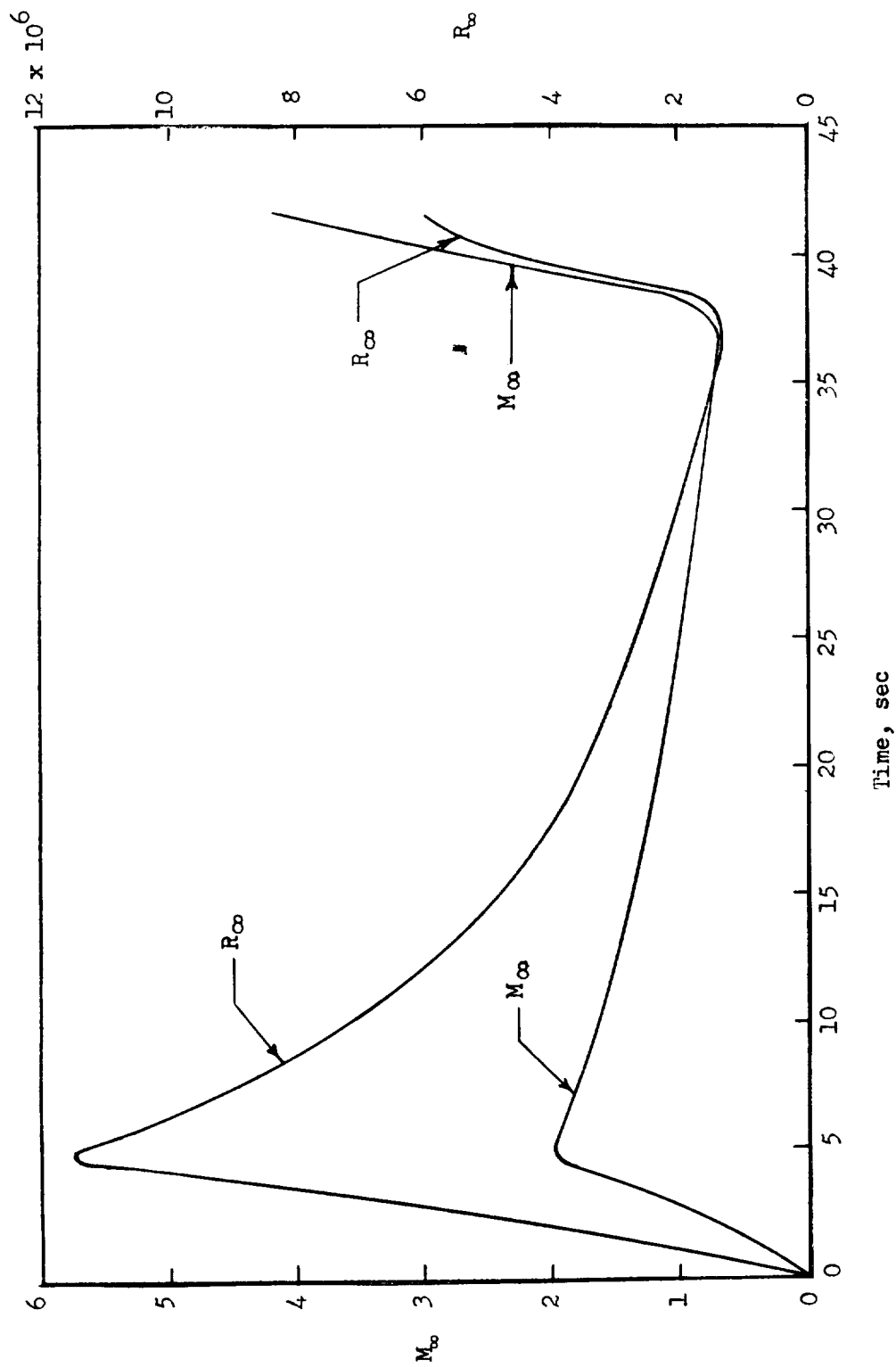
L-171

L-1711

Figure 9.- Free-stream Mach number and free-stream Reynolds number per foot for model flight trajectory.
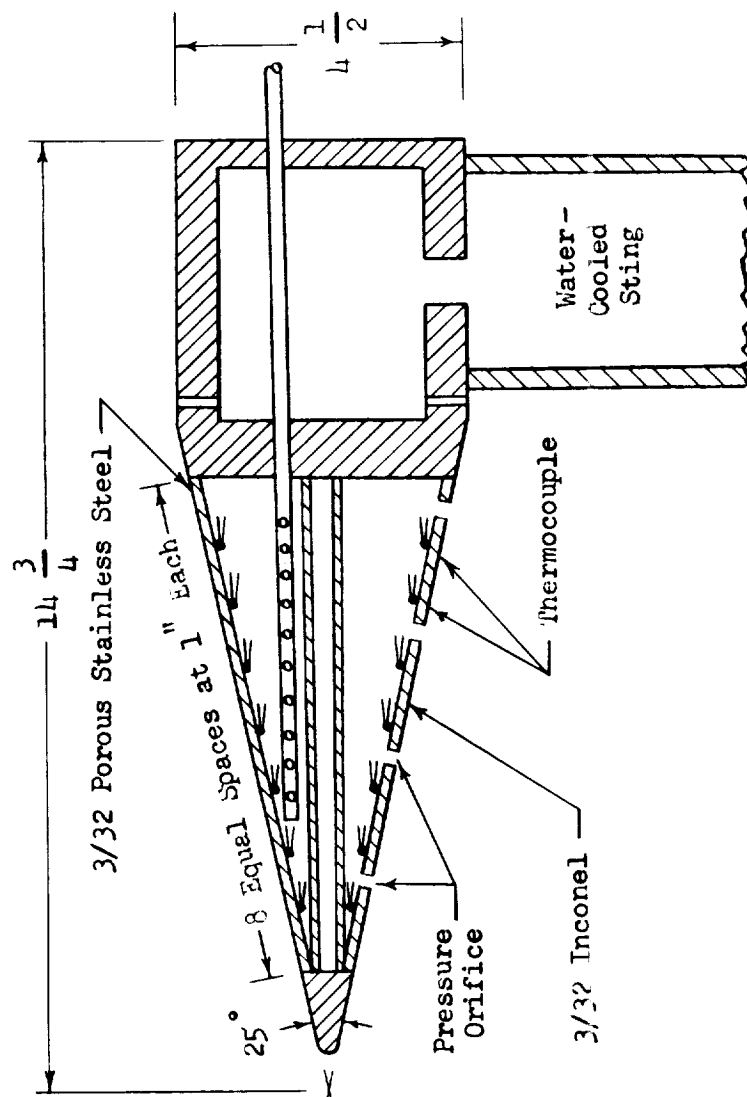
Figure 10.- Sketch of ground-tests model showing construction details and location of instrumentation. All dimensions are in inches.

L-1711

Figure 11.- Photograph of ground-tests model and sting.   L-59-2492

Model ———

Jet

Pressure
Gage

Pressure
Regulator

Coolant
Supply

Solenoid Valve ——

Thermocouple

Flow Meter ——

Figure 12.- Schematic diagram of ground-tests model and cooling system.

L-1711

(a) 40.5 seconds.

(b) 41.0 seconds.

Distance from nose tip, in.
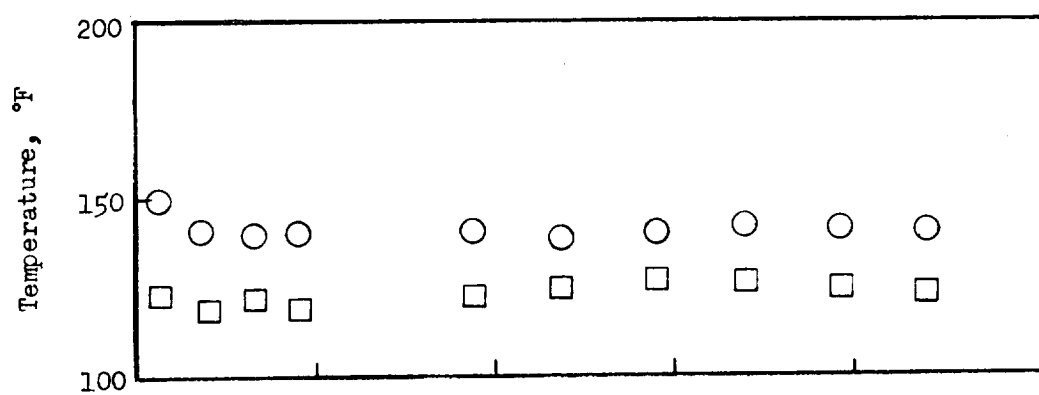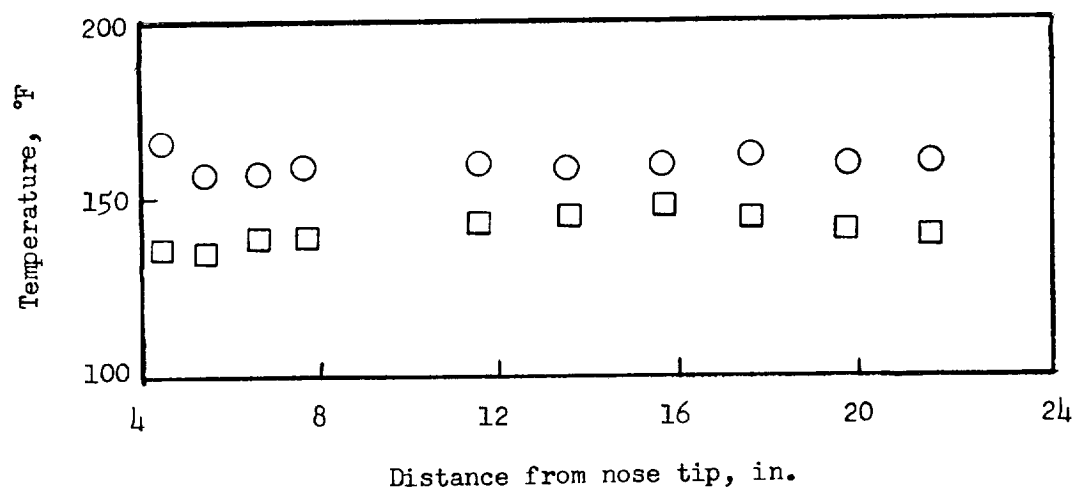
(c) 41.5 seconds.

Figure 13.- Temperature distribution along both the solid and porous conical halves for several times during flight test.
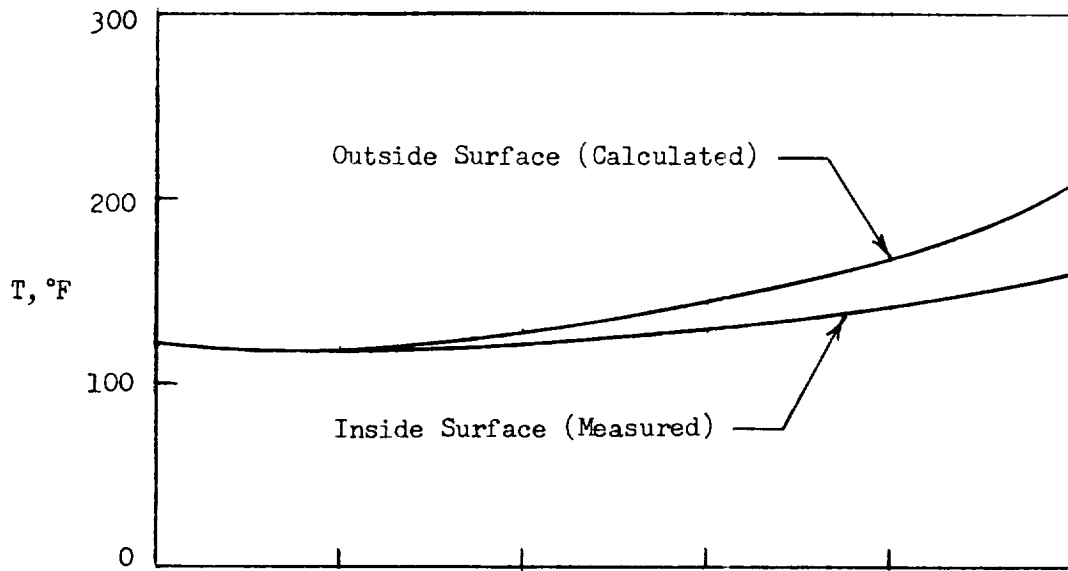
(a) Temperature at station 18 (solid section).
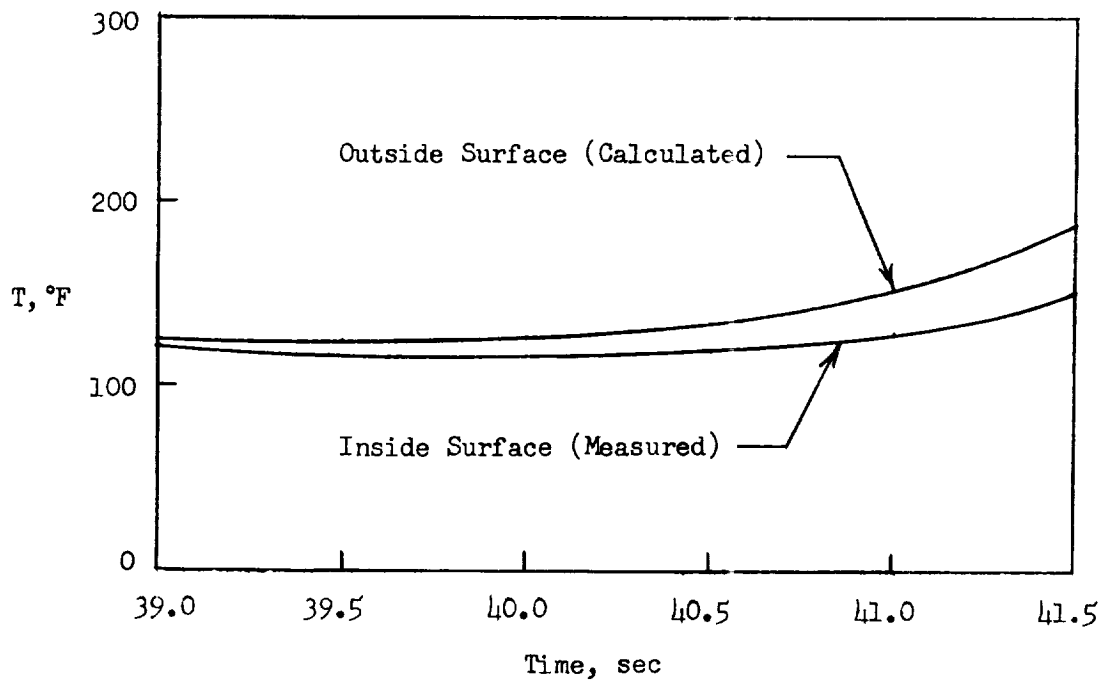
(b) Temperature at station 7 (porous section).

Figure 14.- Time histories of typical outside and inside skin temperature on both the solid and porous sections of flight model cone.
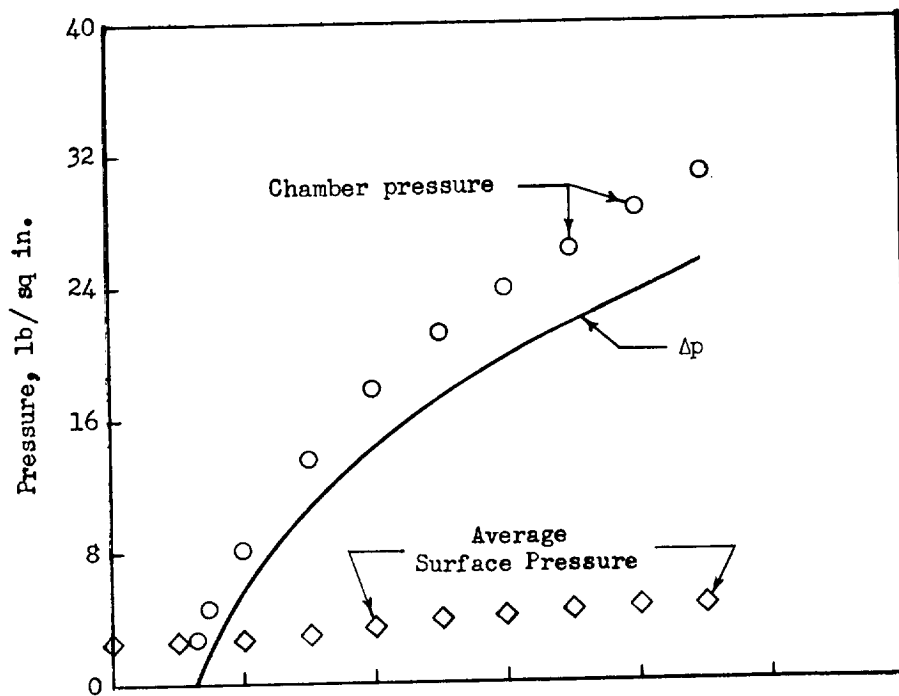
(a) Chamber pressure Δp and surface pressure on model cone.
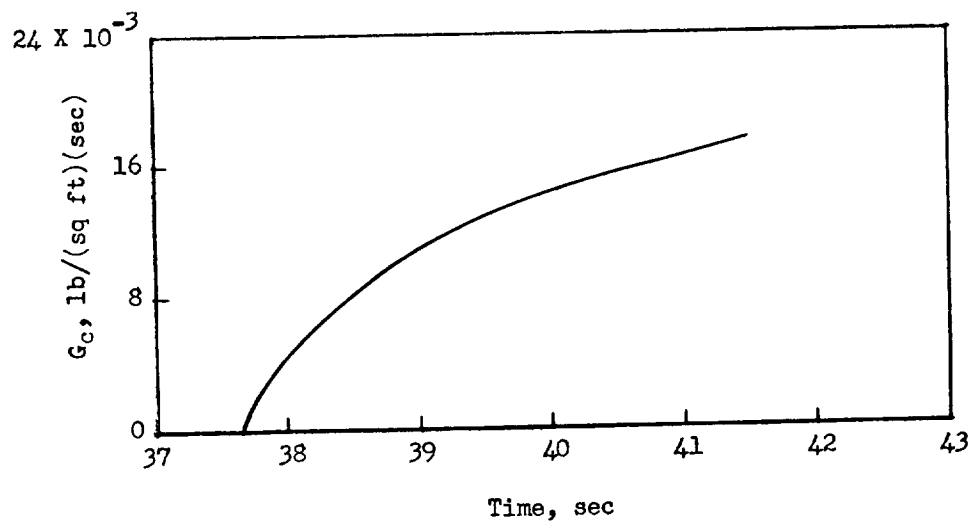
(b) Mass flow rate of nitrogen coolant.

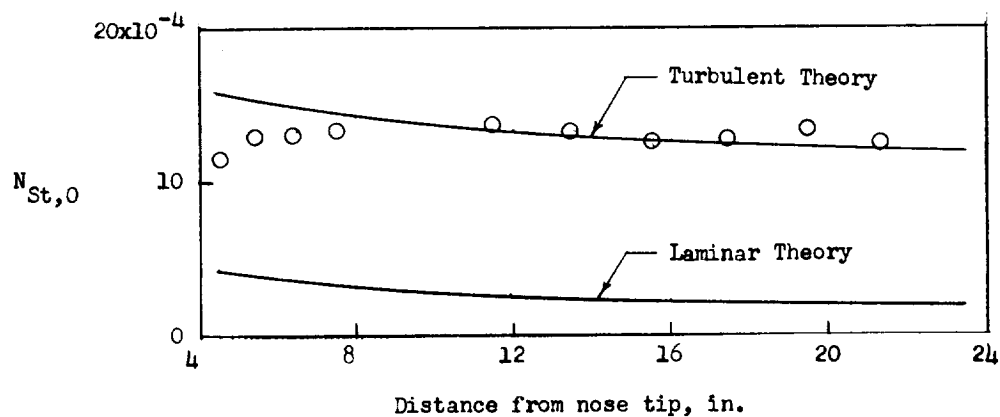Figure 15.- Flight model pressures and coolant mass flow rate as a function of time.
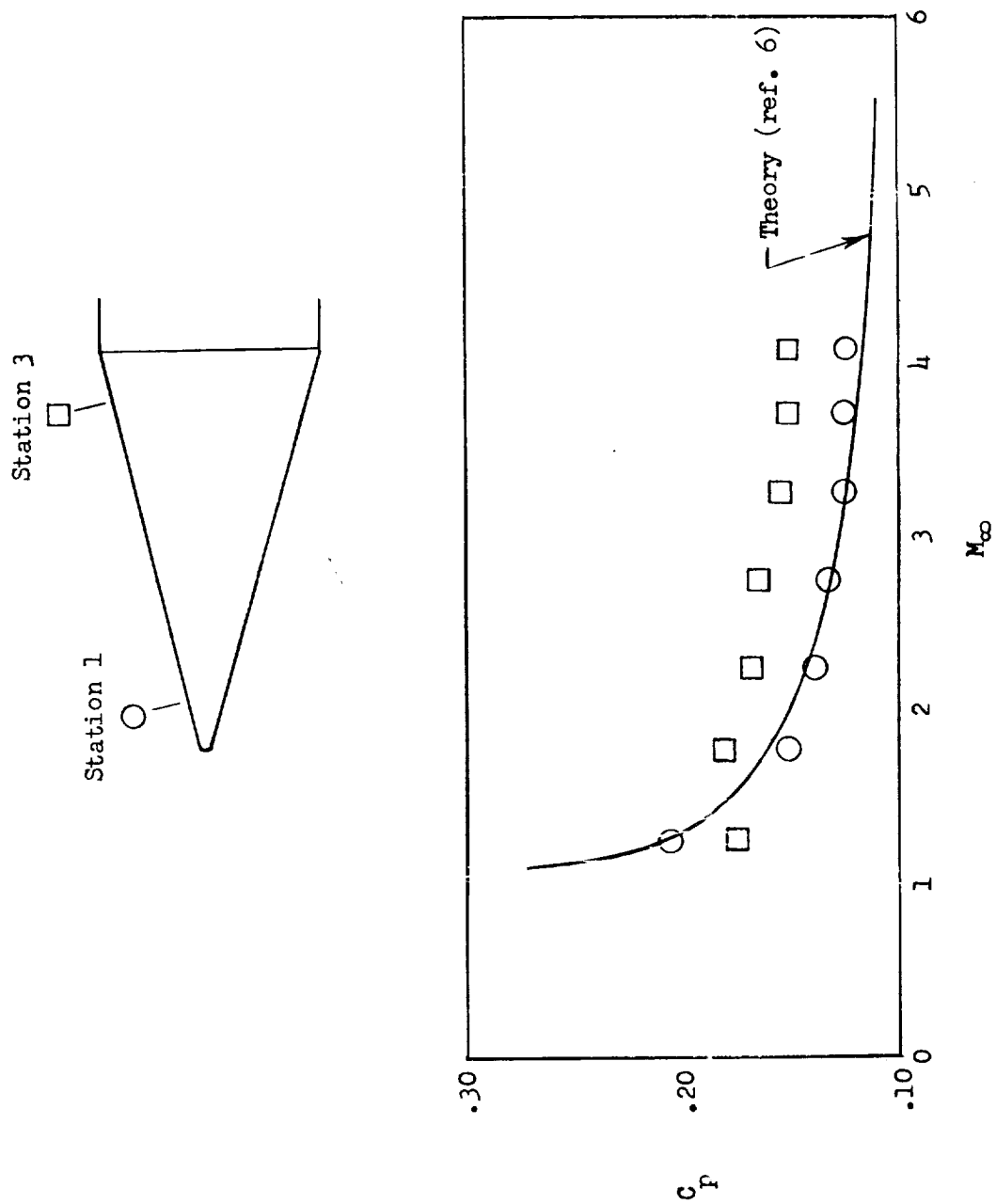
Figure 16.- Pressure coefficient as a function of free-stream Mach number for flight-test cone.
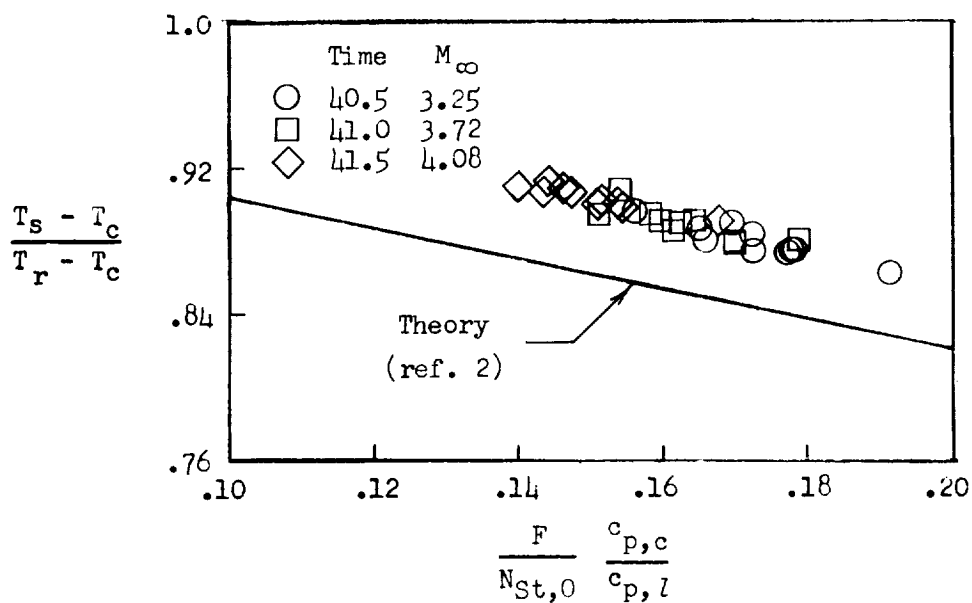
L-1711
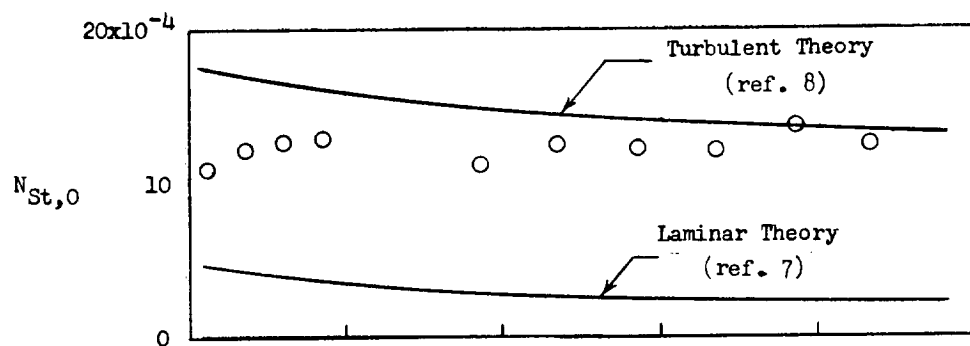
(a) 40.5 seconds; $M_\infty = 3.25$.
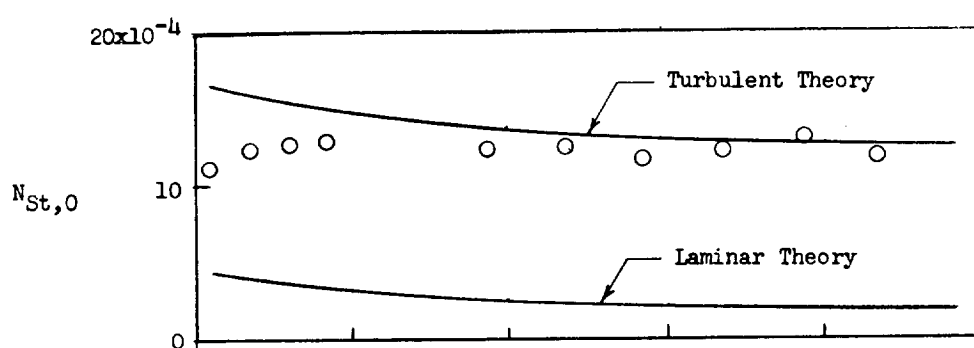
(b) 41.0 seconds; $M_\infty = 3.72$.

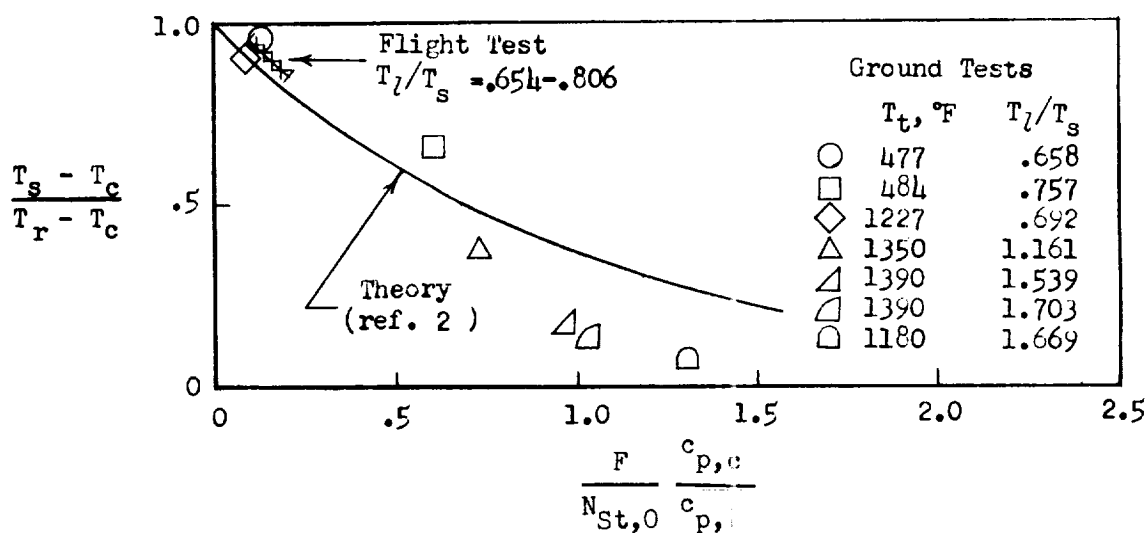(c) 41.5 seconds; $M_\infty = 4.08$.

Figure 17.- Stanton number variation along model cone for several times during flight test.

(a) Cooling efficiency parameter as a function of flow parameter for flight test.

(b) Cooling efficiency parameter as a function of flow parameter.

Figure 18.- Transpiration-cooling results from ground-tests data and flight-test data.
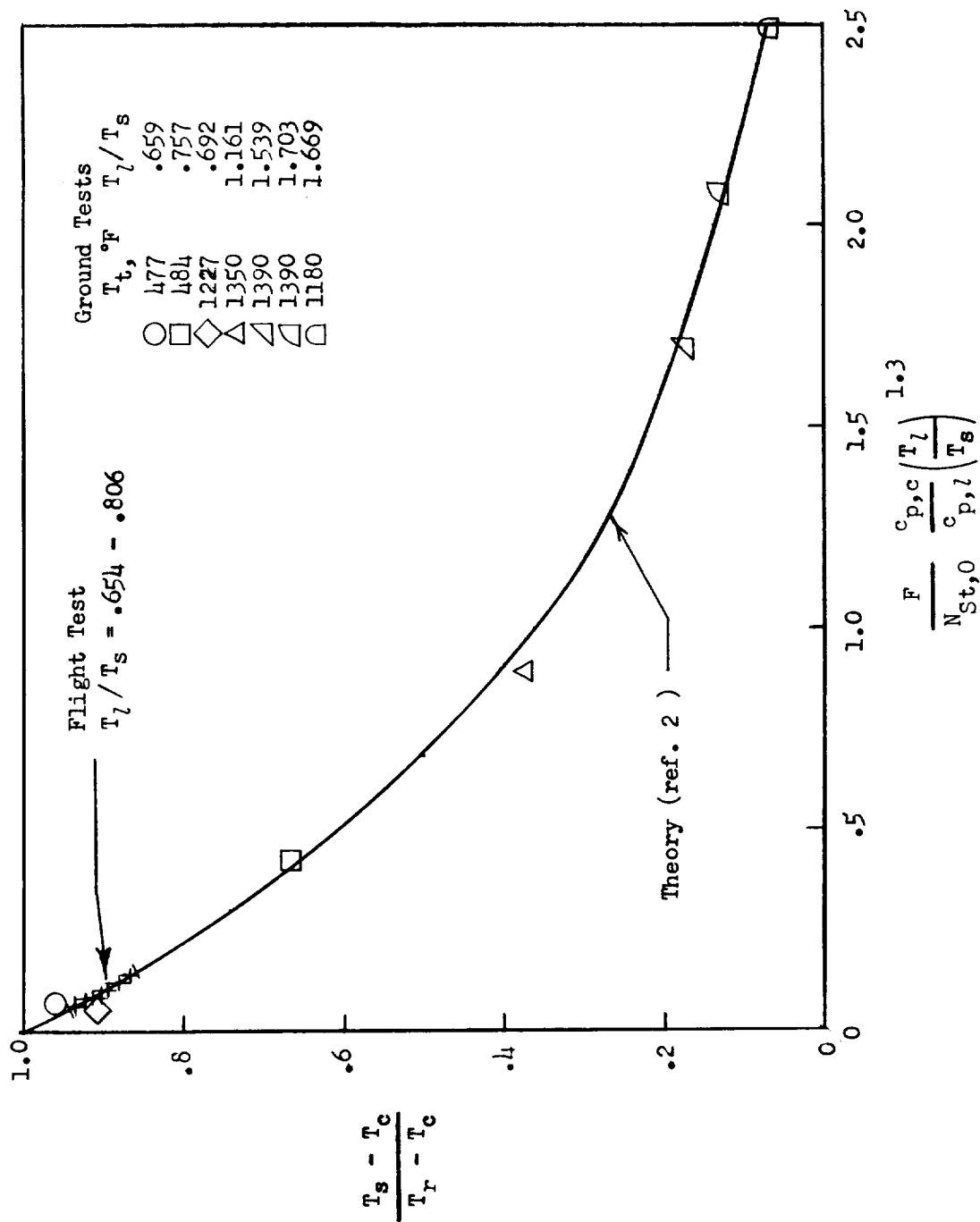
Figure 19.- Transpiration-cooling results from ground-tests data and flight-test data.

L-1711